Joint body wave-surface wave imaging of the Central California Seismic Project region
Final Report, Project #17188

PI Clifford Thurber
University of Wisconsin-Madison
November 28, 2018

Research accomplished

The goal of our project is to contribute to the development of high-resolution compressional and shear wave velocity (Vp and Vs) models for the region of the SCEC Central California Seismic Project, a region termed the Central California Area (CCA). The work we have carried out involves several tasks. (Task 1) One is to merge our previous seismic velocity tomography datasets that cover different parts of the CCA, and integrate them to densely cover the entire CCA. These include both body-wave and surface-wave datasets, the latter from ambient noise. (Task 2) Another more time-consuming task is to further augment the existing datasets in order to provide improved spatial sampling of the region. A key part of this task is to substantially increase the number of S-wave arrivals in the body-wave dataset and expand the coverage of ambient noise correlation functions (ANCFs) for the surface-wave dataset. (Task 3) The final task is to carry out preliminary joint inversions of the enlarged body-wave and surface-wave datasets, and compare the resulting model to the SCEC CCA-06 model. First, we briefly describe the existing body-wave and surface-wave datasets, from which we have extracted data that fall within the CCA. Next, we describe our accomplishments in expanding the datasets. We conclude with a discussion of the preliminary joint inversion results, and suggest future directions for our work.

Task 1: Dataset integration

Several of our previous regional-scale body-wave tomography studies cover part or all of the CCA. These include Thurber et al. (2006) and Zeng et al. (2016) for the greater Parkfield region (Figure 1a), unpublished results for the central California coast region (Figure 1b), Thurber et al. (2009) for Northern California (Figure 1c), and Lin et al. (2010) for all of California (Figure 1d). The data come from different time periods with different station configurations and spatial distributions of earthquakes. We have extracted an optimal, combined dataset from these previous studies, including incorporating all available explosion data within the CCA.

Task 2: Dataset expansion

Even with these large existing body-wave datasets, there is a need for improvement, especially regarding S waves and data coverage in the Great Valley and Sierra Nevada, where permanent network instrumentation has been quite sparse. To that end, we have acquired the Sierra Nevada EarthScope Project (SNEP) dataset, and have completed a two-stage auto-picking procedure on the data. The first stage involves application of an auto-picking method developed by S. Roecker (pers. comm.) that uses an iterative detection-picking-location-repicking strategy. The procedure, known as REST, yields exceptionally high quality P-wave arrivals, and performs reasonably well for S waves. Examples are shown in Figure 4. We focused on earthquakes in the USGS catalog of magnitude 2.5 and above that are within the CCA that occurred during the period of the SNEP deployment.

We have obtained ~14,000 P and ~11,000 S picks from ~600 earthquakes recorded at SNEP stations within CCA. The second stage aims to produce higher quality S-wave arrivals using the kpick algorithm of Rawles and Thurber (2015). Some examples are shown in Figure 5. We have included data from other temporary and permanent stations within CCA in the same time period, including 18 TA stations, during the final phase of revised detection and auto-picking with our two-stage procedure. In total, we have assembled a dataset of ~270,000 P-wave arrival times and ~70,000 S-wave arrival times. The entire explosion and quarry blast dataset of Lin et al. (2010) was added to earthquake body-wave dataset. We initially inverted the dataset for a body-wave model using simul2000 (Thurber and Eberhart-Phillips, 1999) for quality control purposes.

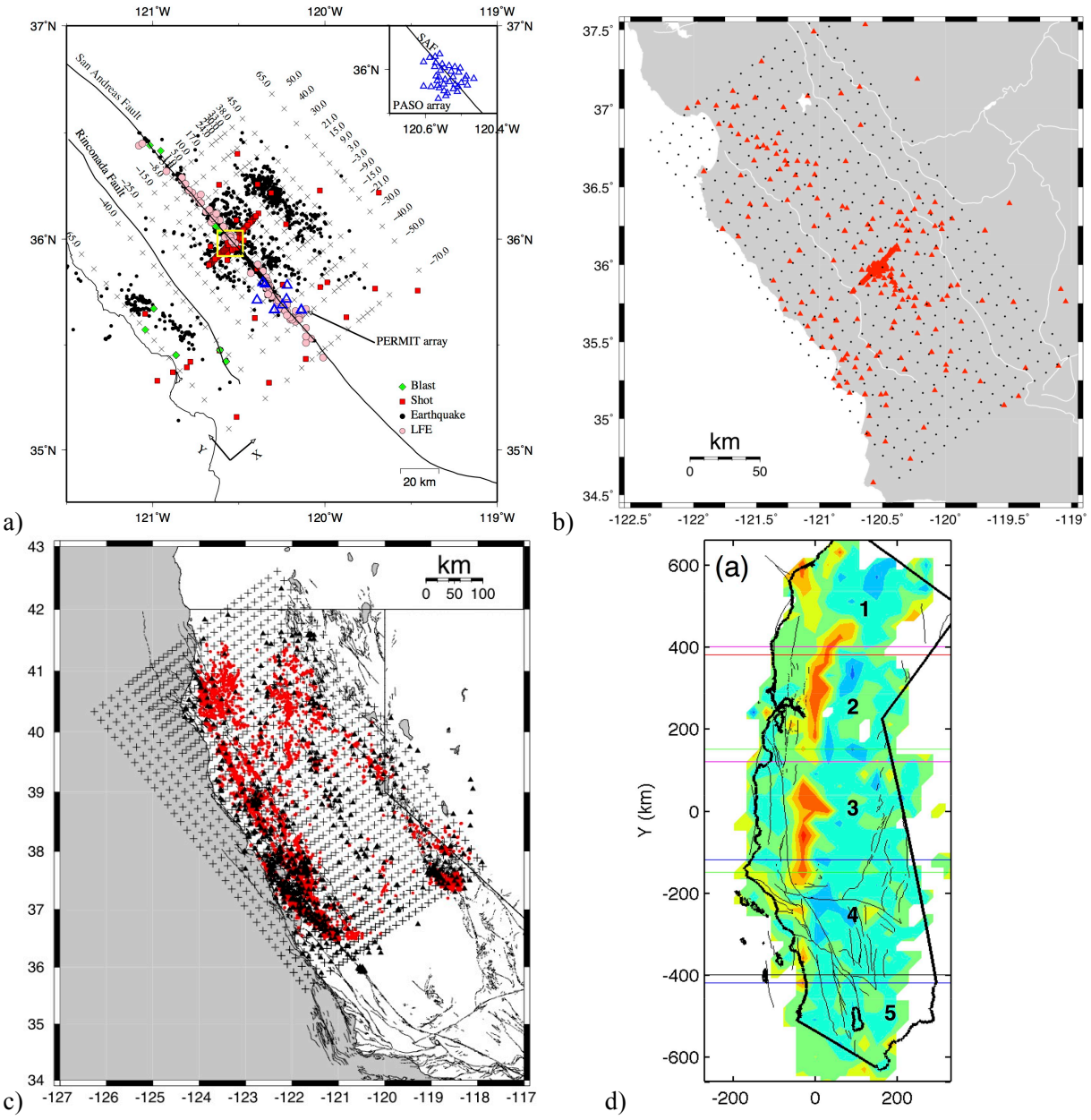

Figure 1. (a) Parkfield model region of Thurber et al. (2006) and Zeng et al. (2016), supported by SCEC and the USGS - Vp and Vs. (b) Region of Thurber's central California coast model, supported by PG&E - Vp and Vs. (c) Northern California model region of Thurber et al. (2009), supported by the USGS - Vp only. (d) Statewide model regions of Lin et al. (2010), supported by the USGS - Vp and minimal Vs.

For the surface-wave dataset, we have assembled a massive set of continuous data for stations that cover the CCA region. The temporary array stations were deployed at different times, so we have gathered ~6 months to 2 years of continuous data from all permanent network stations for time periods that overlap with each temporary deployment. We used the same temporal and spectral normalization factors for all components of a three-component station in order to preserve the relative amplitudes between the components (Lin et al., 2014). We performed additional quality-control checks for clock errors, polarity flips, etc.

For Rayleigh-wave tomography, we used RR, RZ, ZR and ZZ components of noise cross-correlations using all stations in the same time period. We retrieved group velocity dispersion measurements at periods ~4 s to ~18 s using the Automatic Frequency-Time Analysis method (Bensen et al. 2007; Lin et al. 2008). The measurements at each period were inverted for 2D group velocity maps at a node spacing of 0.2° using the 2D Fast Marching surface-wave tomography method (Rawlinson and Sambridge, 2004). Examples are shown in Figure 2. For each horizontal node, we inverted the group velocity dispersion for a vertical Vs profile using the surf96 method (Herrmann, 2013), thus, assembling a 3D Vs model.

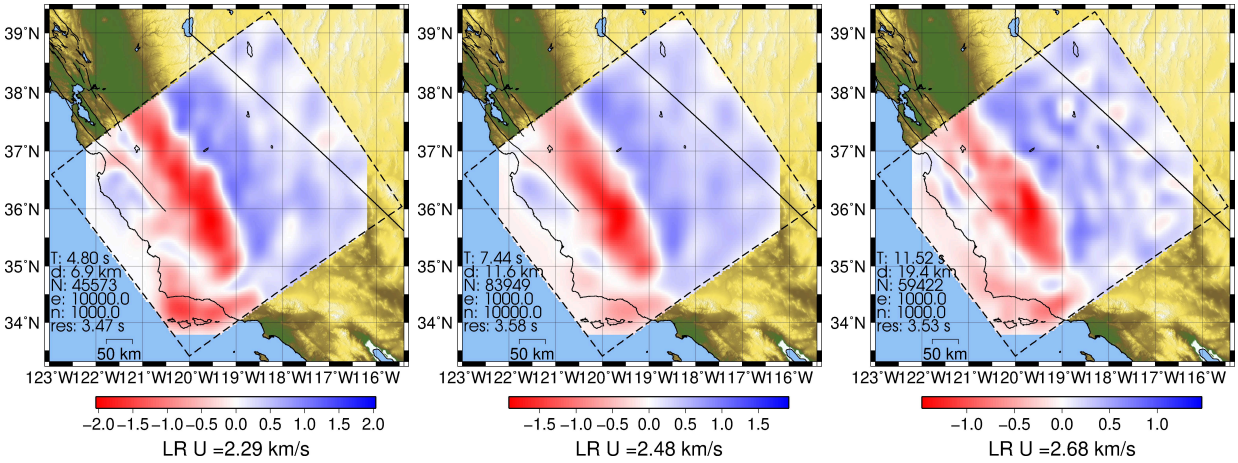

Figure 7. Representative Rayleigh wave group velocity maps at periods of (left) 4.8 s, (center) 7.4 s, and (right) 11.5 s. Note the low group velocities in the Great Valley and high group velocities in the Sierra Nevada Mountains.

Task 3: Joint inversions

For the preliminary joint inversion using the Fang et al. (2016) method, we used the entire body-wave dataset (earthquakes and explosions/quarry blasts) supplemented by pick differential times and approximately half of the surface-wave dispersion dataset. The latter limitation was due to an as-of-yet unidentified memory issue with the joint inversion code for our extremely large dataset. The grid spacing was 0.2° horizontally and vertical nodes were at depths of -1, 0, 1, 2, 4, 6, 8, 10, 12, 15, 20, 25 and 35 km (with respect to the WGS84 depth of 0). We used two different initial models, a standard regional 1D velocity model and a 3D model assembled with Vp from Lin et al. (2010) and Vs from our surface-wave tomography, to test the robustness of the inversion. For the 1D initial model, in 9 iterations, the body-wave and surface-wave travel-time misfits decreased from ~0.64 s and ~14.1 s to ~0.28 s and ~3.95 s, respectively. For the 3D initial model, the corresponding initial misfits were lower, ~0.49 s and ~8.2 s, and decreased further to ~0.27 s and ~3.6 s, respectively, over the same number of iterations. We compared our preliminary Vp and Vs model results to the CCA-06 Vp and Vs models, extracted using UCVM (Small et al., 2016). A map in Figure 3a shows the locations of the representative cross-sections that are presented in Figure 3b for Vp and Figure 3c for Vs. In general, there is excellent agreement between all the velocity models.

Summary and recommendations

In summary, we have assembled datasets of earthquake and explosion body-wave arrival times from multiple previous studies in the CCA. We expanded the P-wave and S-wave datasets by adding picks from records of the largest temporary deployment in the Sierra Nevada, SNEP, along with other temporary and permanent stations operating in the CCA. We have retrieved multi-component ANCFs from nearly all temporary and permanent stations deployed in the CCA. We have extracted Rayleigh-wave dispersion measurements from the ANCFs and inverted them for group velocity maps at periods

~4.3 s to ~16 s. These data have been used in preliminary joint inversions, and the resulting models have been compared to the SCEC CCA-06 model. The comparisons are quite favorable.

There are significant opportunities for future work at further improving the 3D P- and S-wave velocity models. In our work on multi-component ambient noise cross-correlations, we have assembled a large dataset of TT component ANCFs that provide Love-wave dispersion information. The non-uniform spatial distribution of three-component stations in the CCA prevents us from inverting for Love wave group velocity maps effectively, unlike in the southern California region (Zigone et al., 2015). However, the inversion method of Fang et al. (2016) allows one to express both Rayleigh and Love wave group and phase velocity dispersion directly in terms of a 3D Vs model, facilitating the joint inversion of a smaller Love wave dataset with a larger Rayleigh wave dataset. Similarly, one could also add Rayleigh-wave ellipticity measurements on the three-component stations to the joint inversion (Lin et al., 2014; Muir and Tsai, 2017). These two additions would be expected to improve the resolution of the shallow structure. Perhaps most importantly, we have carried out further processing of the ambient noise data to extract phase velocity information. We find that inversions for phase velocity maps result in models with much lower misfits, < 1.5 s, compared to the group velocity map inversions, > 3 s. Joint inversions including the phase velocity information should result in better-constrained 3D models for Vs. We also note that any further effort by SCEC in 3D waveform tomography for the CCA will benefit from our ANCF dataset, which is significantly larger that the dataset used by En-Jui Lee and co-workers to create the CCA-06 model. Our models should also be evaluated as potential starting models for future full waveform tomography efforts in this region.

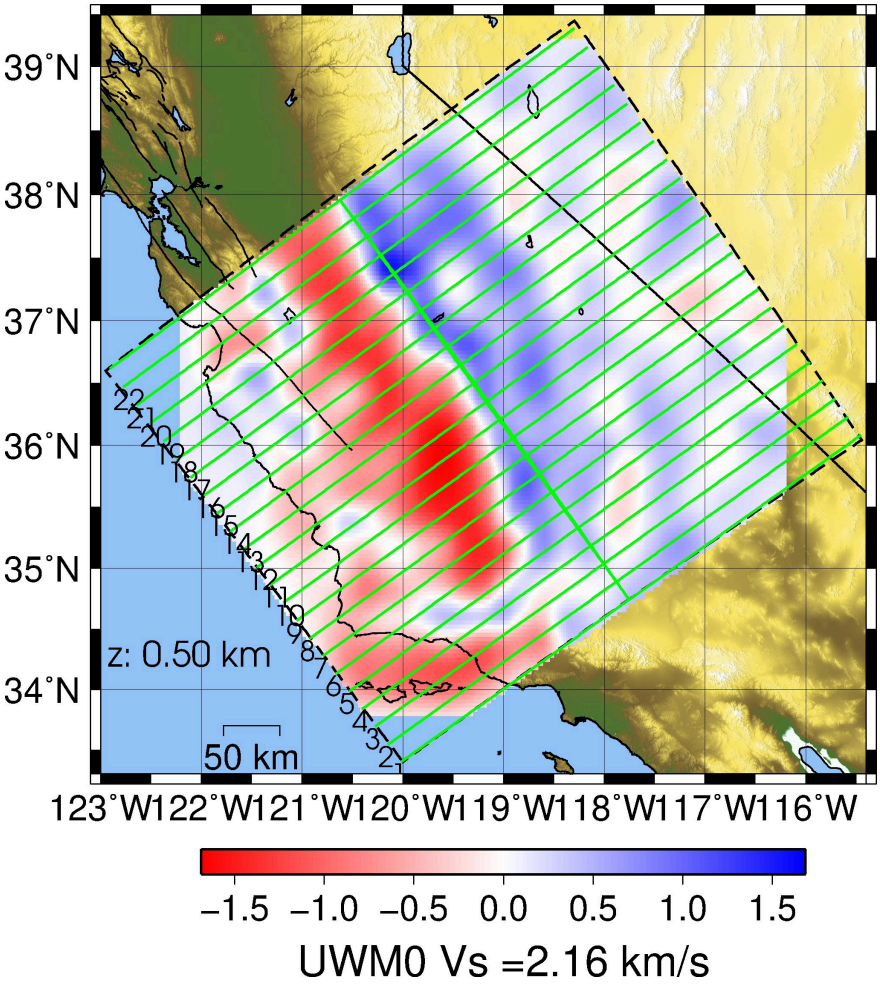

Figure 3a. Map of the positions of the cross-sections through our joint inversion models compared to the SCEC CCA-06 model, shown in Figure 9 for Vp and Figure 10 for Vs for profiles 5-5', 10-10', 15-15', and 20-20'. The velocity model at a depth of 0.5 km, shown as perturbations in km/s about a mean of 2.16 km/s, is from an inversion of the surface-wave data only.

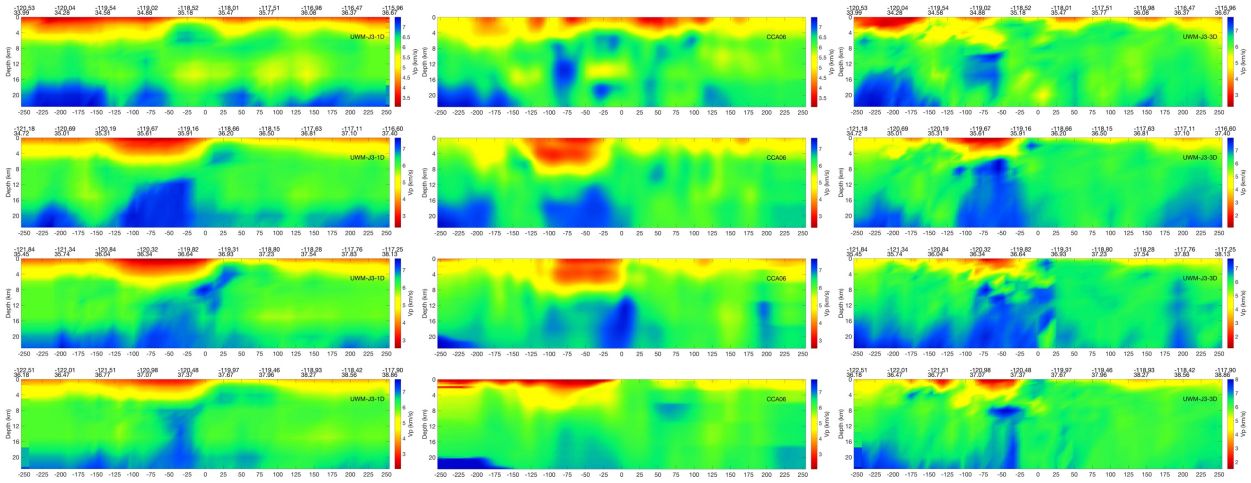

(a) (b) (c)

Figure 3b. Representative cross-sections through our new joint-inversion Vp models compared to the SCEC CCA-06 Vp model along the same profiles shown in Figure 8. (a) Joint inversion Vp model cross-sections, 1D initial model. (b) SCEC CCA-06 Vp model cross-sections. (c) Joint inversion Vp model cross-sections, 3D initial model. Top row: profile 5-5'. Second row: profile 10-10'. Third row: profile 15-15'. Fourth row: profile 20-20'. Note that some apparent discontinuities in the 3D panels arise from interpolating from the N-S/E-W oriented grid in the joint inversion to SW-NE cross-sections.

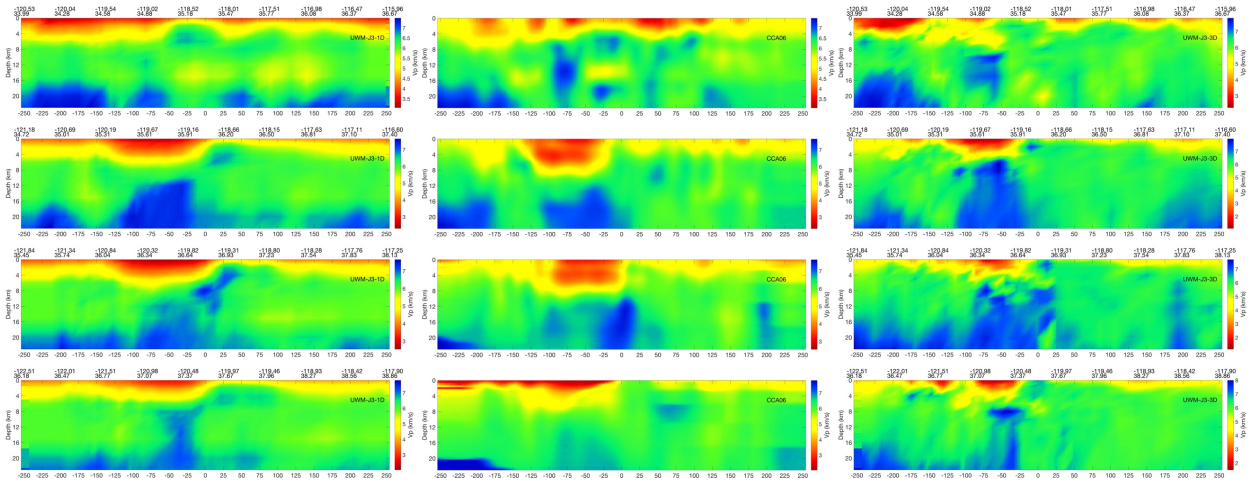

(a) (b) (c)

Figure 3c. Representative cross-sections through our new joint-inversion Vs models compared to the SCEC CCA-06 Vs model. (a) Joint inversion Vs model cross-sections, 1D initial model. (b) SCEC CCA-06 Vs model cross-sections. (c) Joint inversion Vs model cross-sections, 3D initial model. Top row: profile 5-5'. Second row: profile 10-10'. Third row: profile 15-15'. Fourth row: profile 20-20'. Note that some apparent discontinuities in the 3D panels arise from interpolating from the N-S/E-W oriented grid in the joint inversion to SW-NE cross-sections.

References

Bensen, G. D., M. H. Ritzwoller, M. P. Barmin, A. L. Levshin, F.-C. Lin, M. P. Moschetti, N. M. Shapiro, and Y. Yang (2007), Processing seismic ambient noise data to obtain reliable broad-band surface wave dispersion measurements, Geophys. J. Int., 169, 1239-1260.

Brocher, T. M. (2008), Key elements of regional seismic velocity models for long period ground motion simulations, J. Seism., 12, 217-221,10.1007/s10950-007-9061-3.

Fang, H., H. Zhang, H. Yao, A. Allam, D. Zigone, Y. Ben-Zion, C. Thurber, and R. D. van der Hilst (2016), A new algorithm for three-dimensional joint inversion of body wave and surface wave data and its application to the Southern California plate boundary region, J. Geophys. Res.: Solid Earth, 121, 3557-3569, doi:10.1002/2015JB012702.

Herrmann, R. B., (2013), Computer programs in seismology: An evolving tool for instruction and research, Seism. Res. Lett., 84, 1081-1088.

Jiang, C., B. Schmandt, S. M. Hansen, S. L. Dougherty, R. W. Clayton, J. Farrell, and F.-C. Lin (2018), Rayleigh and S wave tomography constraints on subduction termination and lithospheric foundering in central California, Earth Planet Sci. Lett., 488, 14-26, doi: 10.1016/j.epsl.2018.02.009.

Lin, F.-C., M. P. Moschetti, and M. H. Ritzwoller (2008), Surface wave tomography of the western United States from ambient seismic noise: Rayleigh and Love wave phase velocity maps, Geophys. J. Int., 173, 281-298.

Lin, F.-C., V. C. Tsai, and B. Schmandt (2014), 3-D crustal structure of the western United States: application of Rayleigh-wave ellipticity extracted from noise cross-correlations, Geophys. J. Int., 198, 656-670.

Lin, G., C. H. Thurber, H. Zhang, E. Hauksson, P. M. Shearer, F. Waldhauser, T. M. Brocher, and J. Hardebeck (2010), A California statewide three-dimensional seismic velocity model from both absolute and differential times, Bull. Seism. Soc. Am., 100, 225-240.

Maeda, N. (1985), A method for reading and checking phase times in auto-processing system of seismic wave data, Zisin, 38, 365-379.

Muir, J. B., and V. C. Tsai (2017), Rayleigh-Wave H/V via noise cross correlation in Southern California, Bull. Seism. Soc. Am., 107, 2021-2027, doi: 10.1785/0120170051

Rawles, C., and C. Thurber (2015), A nonparametric method for automatic determination of P-wave and S-wave arrival times: Application to local microearthquakes, Geophys. J. Int., 202, 1164-1179, doi:10.1093/gji/ggv218.

Rawlinson, N. and M. Sambridge (2004), Wavefront evolution in strongly heterogeneous layered media using the fast marching method, Geophys. J. Int., 156, 631-647.

Small, P., D. Gill, P. J. Maechling, R. Taborda, S. Callaghan, T. H. Jordan, G. P. Ely, K. B. Olsen, and C. A. Goulet (2017), The SCEC Unified Community Velocity Model software framework, Seism. Res. Lett., 88, doi:10.1785/0220170082.

Tape, C., A. Plesch, J. H. Shaw, and H. Gilbert (2012), Estimating a continuous Moho surface for the California Unified Velocity Model, Seism. Res. Lett., 83, doi: 10.1785/0220110118.

Thurber, C., H. Zhang, F. Waldhauser, J. Hardebeck, A. Michael, and D. Eberhart-Phillips (2006), Three-dimensional compres- sional wavespeed model, earthquake relocations, and focal mechanisms for the Parkfield, California, region, Bull. Seis- mol. Soc. Am., 96, S38-S49, doi:10.1785/0120050825.

Thurber, C., H. Zhang, T. Brocher, and V. E. Langenheim (2009). Regional three-dimensional seismic velocity model of the crust and uppermost mantle of northern California, J. Geophys. Res., 114, B01304, doi 10.1029/2008JB005766.

Zeng, X., C. H. Thurber, D. R. Shelly, R. M. Harrington, E. S. Cochran, N. L. Bennington, D. E. Peterson, B. Guo, and K. McClement (2016), Three-dimensional P- and S-wave velocity structure and low-frequency earthquake locations in the Parkfield, California region, Geophys. J. Int., 206, 1574-1585. doi: 10.1093/gji/ggw217.

Zhang, H., M. Maceira, P. Roux, and C. Thurber (2014), Joint inversion of body-wave arrival times and surface-wave dispersion for three-dimensional seismic structure around SAFOD, Pure Appl. Geophys., 171, doi:10.1007/s00024-014-0806-y.

Zigone, D., Y. Ben-Zion, M. Campillo, and P. Roux (2015), Seismic tomography of the Southern California plate boundary region from noise-based Rayleigh and Love waves, Pure Appl. Geophys., 172, 1007-1032.

Publications

Thurber, C. H., A. Nayak, H. Fang, X. Zeng, and H. Zhang, Tomographic imaging of the Central California crust with multiple methods, SSA Annual Meeting, Miami, FL, May 2018.

Nayak, A., C. H. Thurber, H. Fang, X. Zeng, and H. Zhang, Surface-wave and body-wave tomography for central California, AGU Fall Meeting, December 2018.